NeuroImage: Clinical 32 (2021) 102835

Contents lists available at ScienceDirect

NeuroImage: Clinical

journal homepage: www.elsevier.com/locate/ynicl

Hyperglycemia associated with acute brain injury in neonatal encephalopathy

Emily W.Y. Tam [a,b,*], Daphne Kamino [b], Anwar S. Shatil [b], Vann Chau [a], Aideen M. Moore [a], Rollin Brant [c], Elysa Widjaja [a,b,d]

[a] Department of Paediatrics, The Hospital for Sick Children and the University of Toronto, Toronto, ON, Canada
[b] Neurosciences and Mental Health Program, Hospital for Sick Children Research Institute, Toronto, ON, Canada
[c] Department of Statistics, The University of British Columbia, Vancouver, BC, Canada
[d] Department of Radiology, The Hospital for Sick Children and the University of Toronto, Toronto, ON, Canada

ARTICLE INFO

Keywords:
Hypoglycemia
Hyperglycemia
Neonatal encephalopathy
Diffusion tensor imaging

ABSTRACT

Objective: To identify how alterations in glucose levels are associated with regional brain injury in neonatal encephalopathy.
Methods: This was a prospective cohort study of 102 newborns with neonatal encephalopathy, with continuous glucose monitoring for 72 h. 97 (95%) completed 72 h of therapeutic hypothermia. Brain imaging around day 5 of life included diffusion tensor imaging and MR spectroscopy. Regions of interest were placed for both DTI and MR spectroscopy, and tractography of the optic radiation and corticospinal tract were evaluated. Linear regression models related each MR metric with minimum and maximum glucose values during each day of life, adjusting for 5-minute Apgar scores and umbilical artery pH.
Results: Higher maximum glucose levels on the first day of life were associated with widespread changes in mean diffusivity in the anterior and posterior white matter, splenium of the corpus callosum, lentiform nucleus, pulvinar nucleus of the thalamus, posterior limb of the internal capsule, and optic radiations, thus including regions traditionally associated with hypoxia–ischemia or hypoglycemia. No associations were found between lower minimum glucose levels and DTI changes in any regions tested, or between glucose levels and MR spectroscopy.
Conclusions: In this cohort of neonatal encephalopathy with therapeutic hypothermia, higher maximal glucose on the first day of life was associated with widespread microstructural changes, but lower minimum glucose levels were not associated with changes in any of the regions tested. Long-term follow-up will determine if imaging findings translate to long-term outcomes.

1. Introduction

Neonatal encephalopathy is a clinical syndrome of brain dysfunction that occurs in 1–6 per 1000 live births and is most commonly due to hypoxic-ischemic encephalopathy (HIE), resulting in high rates of morbidity and mortality. Therapeutic hypothermia has resulted in reduction in brain injury and improved outcomes (Jacobs et al., 2013), although high rates of injury and long-term developmental impairment remain. Importantly, brain MRI remains predictive for outcomes (Sanchez Fernandez et al., 2017).

Other etiologies also contribute to neonatal encephalopathy and brain injury, including one third demonstrating hypoglycemia (Wong et al., 2013). Isolated neonatal hypoglycemia has been associated with brain injury in the posterior cortical grey and white matter, as well as the pulvinar nucleus of the thalamus (Barkovich et al., 1998; Wong et al., 2013), associated with adverse outcomes (McKinlay et al., 2017). Combined with HIE, neonatal hypoglycemia continues to demonstrate this specific injury (Wong et al., 2013), while worsening HIE-related brain injury (Tam et al., 2012).

The impact of therapeutic hypothermia on glycemia is only recently coming to light. First, it is unclear how hypothermia has impacted the relationship between hypoglycemia and brain injury. In addition, recent

Abbreviations: CGM, continuous glucose monitoring; DTI, diffusion tensor imaging; FA, fractional anisotropy; MD, mean diffusivity; ROI, region of interest; NAA, N-acetylaspartate; Cho, total choline; FDR, false discovery rate.

* Corresponding author at: Hospital for Sick Children, 555 University Ave, Toronto, ON M5G 1X8, Canada.
E-mail address: emily.tam@utoronto.ca (E.W.Y. Tam).

https://doi.org/10.1016/j.nicl.2021.102835
Received 11 June 2021; Received in revised form 18 September 2021; Accepted 20 September 2021
Available online 28 September 2021

studies have reported an increased incidence of hyperglycemia in the context of hypothermia (Al Shafouri et al., 2015; Chouthai et al., 2015). We have recently reported incidences of hyperglycemia in over half of newborns undergoing therapeutic hypothermia in a subset of this now completed cohort (Pinchefsky et al., 2019). While the contribution of hyperglycemia to worsening brain injury and neurological outcomes is better studied in other patient populations, including adult critical illness (Godoy et al., 2010), adult stroke (Parsons et al., 2002; Saqqur et al., 2015), and prematurity (Auerbach et al., 2013; Slidsborg et al., 2018), there is emerging evidence for worsening of hypoxic-ischemic brain injury and adverse outcomes after neonatal encephalopathy as well (Basu et al., 2016; Montaldo et al., 2020).

This study aimed to optimize our understanding of the implications of abnormal glycemia in neonatal encephalopathy in the era of therapeutic hypothermia by using continuous glucose monitoring (CGM) in the first three days of life combined with detailed regional brain MRI analyses. We hypothesize that hypoglycemia would continue to be associated with a posterior-predominant brain injury independent of hypoxia–ischemia. While the specific patterns of injury associated with neonatal hyperglycemia are not previously reported, we hypothesize that hyperglycemia would be associated with increased severity of brain injury, as assessed by diffusion tensor imaging (DTI) and chemical shift imaging (CSI), and potentially be associated with its own specific pattern of brain injury.

2. Methods

2.1. Study population

Newborns admitted with neonatal encephalopathy to the Neonatal Intensive Care Unit at the Hospital for Sick Children in Toronto, Canada, between 2014 and 2019 were considered for this prospective cohort study. Newborns were considered eligible if they had abnormal consciousness, in addition to either neonatal seizures or abnormalities in tone or reflexes (Badawi et al., 1998). Newborns were excluded if their gestational age at birth was < 36 weeks or there were suspected or confirmed congenital malformations, inborn errors of metabolism, or congenital infections based on clinical examinations and laboratory studies. In addition, they were excluded if a continuous glucose monitor could not be attached within 6 h of life. Infants both eligible and ineligible for therapeutic hypothermia for hypoxia–ischemia were included in this study. Informed consent was obtained from parents or legal guardians following a protocol approved by The Hospital for Sick Children's Research Ethics Board. Clinical data was collected from the clinical notes transferred from the birth hospital, transport records, and our hospital medical records. Study data were managed using research electronic data capture (REDCap, Vanderbilt University, Tennessee) (Harris et al., 2009) hosted at The Hospital for Sick Children.

2.2. Glucose data

Continuous glucose data was collected using an Enlite™ Sensor (Medtronic Canada, Brampton, Ontario) connected to a blinded Medtronic iPro™2 professional CGM (Medtronic Canada, Brampton, Ontario) inserted into the lateral aspect of the thigh within the first few hours of life for approximately 72 h of continuous glucose monitoring. The CGM stores interstitial glucose concentrations and reports data every 5 min once the data are uploaded to the Medtronic CareLink™ iPro™ software (Medtronic MiniMed, Northridge, California) and calibrated. The measurements from the CGM were blinded and unavailable to clinicians for real-time management, and the patients were managed via clinical intermittent glucose testing as per standard of care. Our institution protocols for HIE include laboratory glucose testing on admission and every 12 h of life. Glucose levels ≤ 2.6 mmol/L are treated with dextrose boluses and increased glucose infusion rates, escalating to glucagon if needed. There is no protocol for management of hyperglycemia and no agreed upon threshold, with treatment left to the discretion of the managing team, including observation, decreased glucose infusion rates, or insulin administration.

All clinically ordered laboratory and point-of-care testing blood glucose values were collected from both the birth hospital and at the Hospital for Sick Children. Only blood glucose values obtained via the gold standard glucose oxidase reaction – including both laboratory-obtained values and bedside testing using the i-STAT (Abbott Laboratories, Abbott Park, Illinois) – were used for CGM calibration. Due to Medtronic CareLinkTM iPro™ software limitations for determining interstitial glucose concentrations < 2.2 and > 22.2 mmol/L (<40 and > 400 mg/dL), interstitial glucose readings initially reported as 2.2 or 22.2 mmol/L were verified or corrected manually using an equation provided by Medtronic to calculate their true interstitial glucose concentrations.

Minimum and maximum glucose values in the first 24 h of life (day 1), between 24 and 48 h of life (day 2), and between 48 and 72 h of life (day 3) were determined using CGM data when available, supplemented by intermittent testing when not available, especially in the first few hours of life prior to CGM insertion.

2.3. MRI data collection

After patients were rewarmed, MRI scans were performed at around day 5 of life on a 3 T or 1.5 T MRI scanner (Siemens Magnetom Prisma or Skyra, or Philips Achieva 3 T or 1.5 T). As these images were obtained for both clinical and research purposes, sedation was used when indicated by the clinical team, using either intravenous midazolam (46% subjects) or oral chloral hydrate (38% subjects). Imaging sequences included diffusion tensor imaging (TR/TE = 8000/86, FOV = 160 mm, slice thickness = 2 mm, 30 directions, matrix = 80x80, b = 700 s/mm^2, Number of signal averages [NSA] = 1, 4.56-minute scan time) and multivoxel 2D ^{1}H-MRS chemical shift imaging (CSI) acquired at the level of basal ganglia, as well as in the frontal and parietal white matter above the lateral ventricles using point-resolved spectroscopy (PRESS) (TR/TE = 2000/144, FOV = 160 mm, slice thickness = 15 mm, flip angle = 90 degree, NEX = 8, voxel size = 80x80 mm, NSA = 8, 4.10-minute scan time). Of note, the DTI parameters were chosen to balance data quality and imaging time in newborn infants, accounting for relatively high water content in newborns compared to adults, and are in line with most prior published DTI studies in newborns (Chau et al., 2009; Tam et al., 2009; Tam et al., 2012).

2.4. Diffusion tensor imaging processing

DTI maps were preprocessed with a customized pipeline, using a combination of software tools, including: (1) The FMRIB software library (Oxford Centre for Functional MRI of the Brain, Oxford, UK), (2) MATLAB (The MathWorks Inc., Natick, MA, USA), (3) Statistical Parametric Mapping (SPM12) (Wellcome Trust Centre for Neuroimaging, London, UK), and (4) Analyze 12.0 (Analyze Direct, Inc., Overland Park, Kansas). All axial DTI images were eddy current and motion corrected by using the Artefact Correction in Diffusion MRI (ACID) toolbox in SPM12 (Mohammadi et al., 2010). To quantify motion on DTI images, translation and rotation motion were assessed. Subjects with translation motion that exceeded 2 mm and rotation motion that exceeded 0.5 degree were excluded. The b0 images were skull stripped using FSL Brain Extraction Tool algorithm with a fractional intensity threshold of 0.4. (Smith et al., 2006) FSL DTI fitting module was used to generate fractional anisotropy (FA) and mean diffusivity (MD) (Behrens et al., 2003). Regions of interest (ROI) were manually drawn in Analyze 12.0 software by an expert research analyst (AS) in 13 bilateral white matter and deep grey structures which were guided by axial FA, b0 and b0-coregistered T2 images (Fig. 1). The anterior, central and posterior white matter ROIs were placed in the plane of centrum semiovale (above the lateral ventricles), and remainder of the ROIs were placed at the level of the

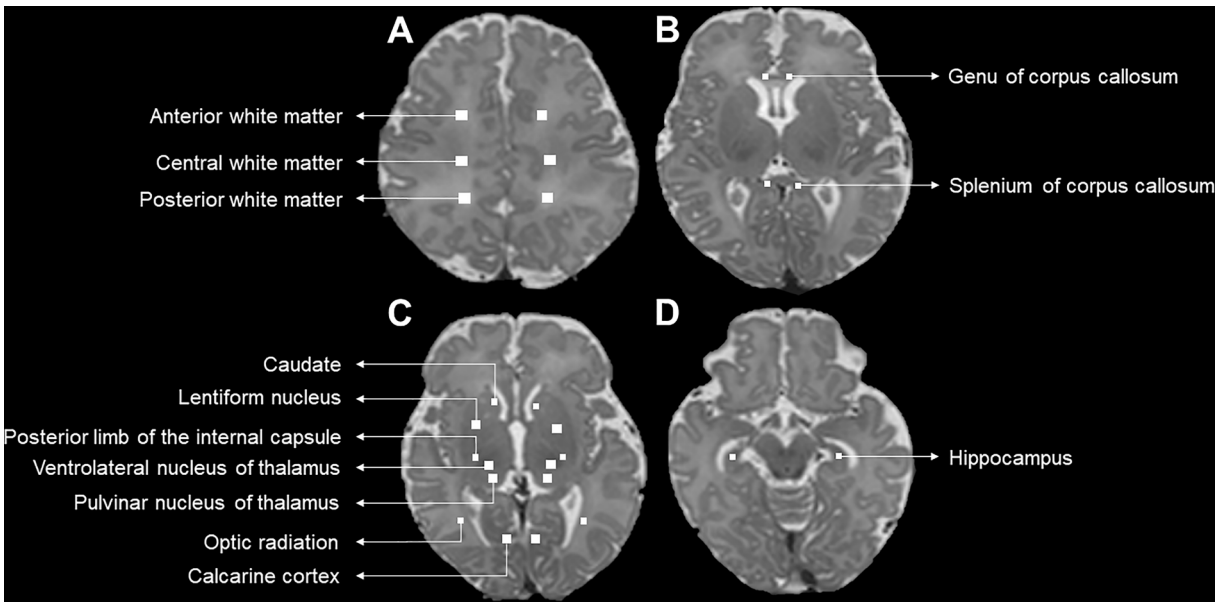

Fig. 1. Regions of interest for diffusion tensor imaging (DTI). Thirteen bilateral regions of interest shown on axial T2-image maps at the levels of (A) the centrum semiovale (above the lateral ventricles); (B and C) the basal ganglia; and (D) midbrain and hippocampus.

basal ganglia (Chau et al., 2009). Finally, mean FA and MD values were extracted using an in-house MATLAB code. Values from left and right hemisphere were averaged for analysis.

2.5. Diffusion tensor tractography

Diffusion tensor data were postprocessed using Diffusion Toolkit and TrackVis software (Ruopeng Wang, Van J. Wedeen, TrackVis.org, Martinos Center for Biomedical Imaging, Massachusetts General Hospital). Fiber Assignment by Continuous Tracking (FACT) algorithm was used to run deterministic white matter fiber bundle tracking. Corticospinal tract fiber tracking (Fig. 2A) was initiated with a seeding ROI in the posterior limb of the internal capsule at the level of the foramen of Monro. Tracts were terminated if the angle between the primary eigenvectors of consecutive voxels exceeded 50 degrees or they did not pass through 2 limiting ROIs at the precentral gyrus and cerebral peduncle. Fiber trajectories of the optic radiation (Fig. 2B) were launched from a ROI drawn on a coronal plane anterior-lateral to the trigone of the lateral ventricle. Fibers passing through a second ROI drawn in a coronal plane posterior to the lateral ventricle were retained as the delineated optic radiation. Later, tract-based diffusion statistics including FA and MD were calculated. Values from left and right hemisphere were averaged for analysis.

2.6. MR spectroscopy data processing

MRS PRESS data were analysed using TARQUIN (Totally Automatic Robust Quantification In NMR) version 4.3.10 in order to suppress the water signal (Carlin et al., 2019; Wilson et al., 2011). The spectra were referenced to a combination of total choline-creatine-NAA-lipids. Due to significant spectral overlap, total N-acetylaspartate (NAA) included a combination of N-acetylaspartate and N-acetylaspartylglutamate, and total choline (Cho) included a combination of glycerophosphocholine and phosphocholine. Lactate was also measured. ROIs were placed at in the anterior, central, and posterior white matter, caudate, lentiform nuclei, thalamus, optic radiations, and calcarine cortex (Fig. 3) (Chau

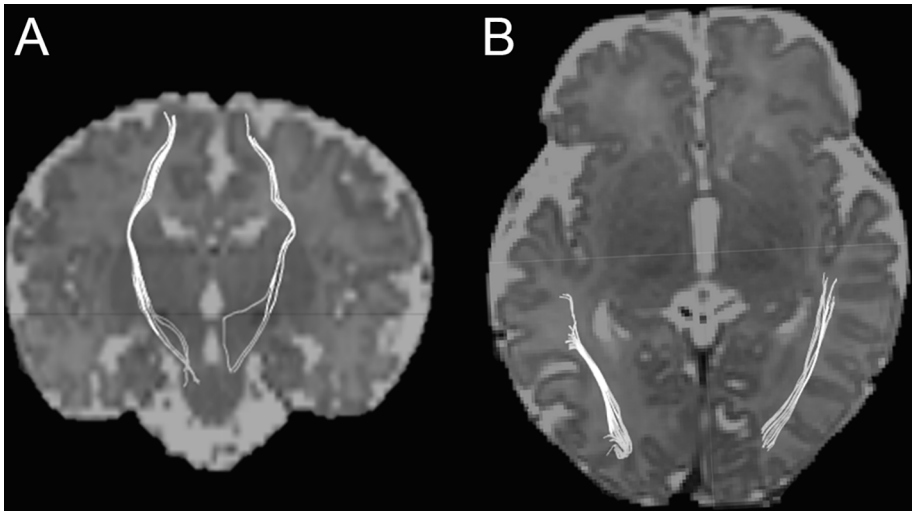

Fig. 2. Diffusion tensor tractography. A. Coronal T2 image demonstrating tractography of the corticospinal tract from the motor cortex to the pons. B. Axial T2 image demonstrating tractography of the optic radiation lateral to the trigone of the lateral ventricle to the calcarine cortex.

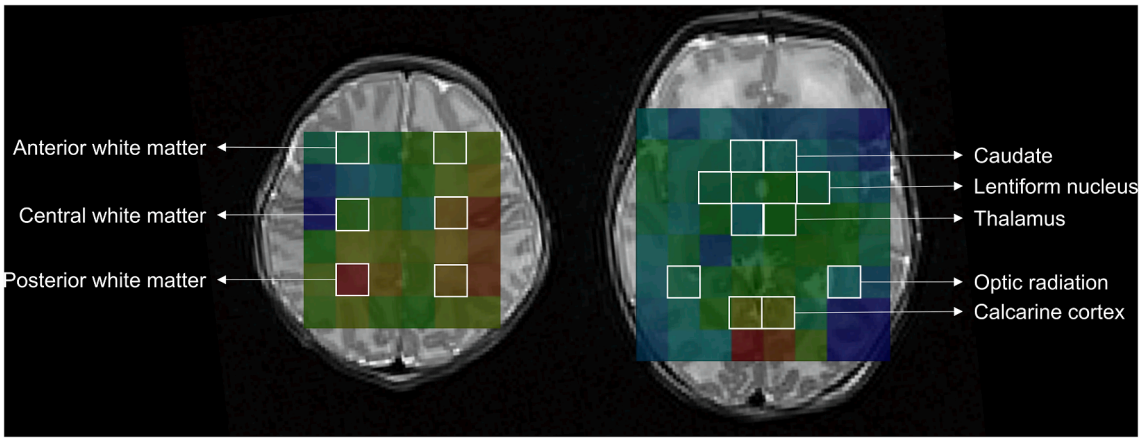

Fig. 3. Regions of interest for MR spectroscopic imaging (MRSI). MRSI superimposed on axial T2-images at the level of the centrum semiovale (left image) and basal ganglia (right image), showing the eight bilateral regions of interest.

et al., 2009). Values from left and right hemisphere were averaged for analysis.

2.7. Statistical analysis

Statistical analyses were performed using Stata 12.1 software (Stata Corporation, College Station, TX). Descriptive statistics were used to describe the study cohort. Each imaging metric, including DTI ROI (FA and MD), diffusion tractography of corticospinal tract and optic radiation (FA and MD) and MRS values (lactate/Cho ratio and the NAA/Cho ratio), was regressed against minimum and maximum glucose values each day of life using multiple linear regression, adjusting for postmenstrual age at time of MRI scan, 5-minute Apgar scores, and umbilical artery pH, to quantitatively control for degree of hypoxic-ischemic insult. To account for the large number of comparisons made, sharpened False Discovery Rate (FDR) q-values were calculated (Anderson, 2008), with significance set to a q-value of 0.05.

3. Results

3.1. Subject demographics

A total of 102 newborns were enrolled with brain MRI completed. Of these, 93 (91%) had adequate quality DTI data and 65 (64%) had adequate spectroscopy data for analysis. Subject demographics are summarized in Table 1, including the neonatal encephalopathy score demonstrating highest severity of clinical encephalopathy in the first 3 days of life. The neonatal encephalopathy score has been validated for prediction of 30-month outcomes, and considers alertness, feeding, tone, respiratory status, reflexes, and seizure activity (Miller et al., 2004). There was no significant difference in the demographics between those with and without completed DTI and MRS studies. Of 93 subjects, 78 (84%) were scanned on a 3 T and 15 (16%) on a 1.5 T field-strength MRI scanner.

Of the 102 subjects, 97 (95%) subjects underwent 72 h of therapeutic hypothermia for presumed hypoxic-ischemic encephalopathy, 4 (4%) were rewarmed early between 3 and 34 h of life, and 1 (1%) did not undergo therapeutic hypothermia due to decision by the clinical team. Of the 4 subjects rewarmed early, 2 were deemed clinically too well to continue hypothermia treatment, 1 was sent to a palliative care home but since survived, and 1 was discontinued due to excessive hemorrhages from disseminated intravascular coagulation.

3.2. DTI regions of interest

The potential utility of minimum glucose values on each day of life in predicting the DTI variables (FA and MD) for each of the ROIs was examined using multiple linear regression adjusting for maximum glucose on the same day, postmenstrual age at time of MRI, 5-minute Apgar scores, and umbilical artery pH. No associations were found between minimum glucose and FA or MD changes in any of the regions of interested tested.

Similarly, the DTI variables (FA and MD) for each of the ROIs were regressed against maximum glucose values on each day of life, adjusting for minimum glucose on the same day, postmenstrual age at time of MRI,

Table 1
Subject demographics. Demographics for the full cohort, as well as those with completed diffusion tensor imaging (DTI) and MR spectroscopy (MRS), expressed as number and proportion, mean ± standard deviation, or median and intraquartile range (IQR). The neonatal encephalopathy score gives one point for each sign of abnormal feeding, alertness, tone, respiratory status, reflexes, and seizures. The highest score in the first 3 days of life is reported.[21]

	Full cohort (N = 102)	DTI complete (N = 93)	MRS complete (N = 65)
Male sex	64 (63%)	60 (65%)	40 (62%)
Gestational age at birth (weeks)	39.6 ± 1.3	39.7 ± 1.3	39.7 ± 1.4
Birthweight (grams)	3361 ± 529	3391 ± 520	3336 ± 523
5-minute Apgar score	4 (IQR 3–6)	4 (IQR 3–6)	4 (IQR 3–6)
Umbilical artery pH	7.01 ± 0.15	7.01 ± 0.16	7.03 ± 0.14
Encephalopathy score			
0/6	0 (0%)	0 (0%)	0 (0%)
1/6	0 (0%)	0 (0%)	0 (0%)
2/6	6 (6%)	5 (5%)	3 (5%)
3/6	14 (14%)	14 (15%)	11 (17%)
4/6	30 (30%)	26 (28%)	20 (30%)
5/6	25 (25%)	25 (27%)	17 (26%)
6/6	27 (26%)	23 (25%)	14 (22%)
Day of life at MRI (days)	5 (IQR 4–5)	5 (IQR 4–5)	5 (IQR 4–5)
Minimum glucose ≤ 2.6 mmol/L	25 (25%)	21(23%)	16 (25%)
Maximum glucose > 8 mmol/L	43 (42%)	37 (40%)	29 (45%)
Minimum glucose on day of life 1 (mmol/L)	3.16 ± 1.32	3.23 ± 1.31	3.18 ± 1.26
Maximum glucose on day of life 1 (mmol/L)	8.38 ± 3.65	8.35 ± 3.61	8.34 ± 3.91
Minimum glucose on day of life 2 (mmol/L)	3.98 ± 2.00	3.96 ± 2.00	3.95 ± 2.31
Maximum glucose on day of life 2 (mmol/L)	7.13 ± 3.93	7.01 ± 3.84	6.89 ± 3.86
Minimum glucose on day of life 3 (mmol/L)	3.64 ± 1.61	3.59 ± 1.66	3.71 ± 1.94
Maximum glucose on day of life 3 (mmol/L)	6.04 ± 2.89	6.02 ± 2.99	6.02 ± 3.38

5-minute Apgar scores, and umbilical artery pH. Maximum glucose values on the first day of life were predictive of decreased MD, but not FA, in the anterior and posterior white matter, splenium of corpus callosum, lentiform nuclei, pulvinar, posterior limb of internal capsules and optic radiations with moderate effect size (Table 2). For example, per 1 mmol/L higher maximum glucose on the first day of life, there is a 1.50 $\times 10^{-5}$mm^2/s lower mean diffusivity in the anterior white matter (FDR sharpened q = 0.04). Higher maximum glucose on the second or third day were not associated with any FA or MD changes. Mean FA and MD metrics in each ROI in the cohort are summarized in Table 4.

3.3. Diffusion tractography

Analyzing tractography in the corticospinal tract and the optic radiation, DTI variables were regressed against minimum and maximum glucose values on each day of life, adjusting for postmenstrual age at time of MRI, 5-minute Apgar scores, and umbilical artery pH. Results are included in Table 3.

Lower minimum glucose on the second day was associated with higher MD in the optic radiation, with moderate effect size. Higher maximum glucose on the first day was associated with lower MD in both the corticospinal tract and optic radiation, with small to moderate effect size; on the second day was associated with lower FA in both corticospinal tract and optic radiation with moderate effect size; and on the third day was associated with lower FA in the optic radiation with moderate effect size. Mean FA and MD metrics of the corticospinal tract and optic radiation tract of the cohort are summarized in Table 4.

3.4. MR spectroscopy

MR spectroscopy variables studied included the lactate/Cho ratio and the NAA/Cho ratio. These variables were regressed against minimum and maximum glucose values on each day of life, adjusting for postmenstrual age at time of MRI, 5-minute Apgar scores, and umbilical

Table 2
Linear regression models of the relationship between maximum glucose (mmol/L) on the first day of life and diffusion tensor imaging metrics, including fractional anisotropy (FA) and mean diffusivity (MD). All models are adjusted for postmenstrual age at time of MRI, minimum glucose on first day of life, 5-minute Apgar scores, and umbilical artery pH. Standardized beta coefficients (β) are included. Significant sharpened q-values are marked with an asterisk.

	FA	β	q-value	MD (10^{-5} mm^2/s)	β	q-value
Anterior white matter	−0.0029	−0.21	0.19	−1.50	−0.31	0.04*
Central white matter	−0.0012	−0.07	0.67	−0.74	−0.16	0.35
Posterior white matter	−0.0021	−0.12	0.51	−2.07	−0.32	0.04*
Genu of corpus callosum	−0.0074	−0.19	0.25	−2.30	−0.27	0.08
Splenium of corpus callosum	−0.0021	−0.07	0.66	−2.33	−0.43	0.001*
Caudate	−0.0005	−0.01	1	−0.90	−0.22	0.19
Lentiform nucleus	0.000008	−0.001	1	−0.87	−0.32	0.04*
Pulvinar nucleus of thalamus	−0.0018	−0.11	0.51	−1.21	−0.38	0.001*
Ventrolateral nucleus of thalamus	0.0013	0.122	0.51	−0.54	−0.19	0.30
Posterior limb of the internal capsule	−0.0029	−0.15	0.38	−1.04	−0.33	0.04*
Optic radiation	−0.0043	−0.25	0.08	−2.44	−0.43	0.001*
Calcarine cortex	0.0009	0.07	0.67	−0.55	−0.17	0.35
Hippocampus	0.0009	0.05	0.74	−0.47	−0.09	0.59

Table 3
Diffusion tensor tractography. Linear regression models of the relationship between minimum and maximum glucose (mmol/L) on each day of life and diffusion tensor tractography metrics, including fractional anisotropy (FA) and mean diffusivity (MD). All models are adjusted for postmenstrual age at time of MRI, 5-minute Apgar scores, and umbilical artery pH. Minimum glucose models adjust for maximum glucose, and vice versa. Standardized beta coefficients (β) are included. Significant sharpened q-values are marked with an asterisk.

	FA	β	q-value	MD (10^{-5} mm^2/s)	β	q-value
Corticospinal tract						
Minimum glucose day 1	0.0044	0.17	0.10	−1.83	−0.23	0.08
Maximum glucose day 1	−0.0003	−0.03	0.60	0.74	−0.26	0.02*
Optic radiation						
Minimum glucose day 1	0.0043	0.15	0.11	−0.10	0.01	0.30
Maximum glucose day 1	−0.0017	−0.17	0.12	−1.67	−0.37	0.001*
Corticospinal tract						
Minimum glucose day 2	0.0046	0.28	0.10	−1.66	−0.33	0.10
Maximum glucose day 2	−0.0041	−0.49	0.008*	0.42	0.16	0.43
Optic radiation						
Minimum glucose day 2	0.0068	0.37	0.08	−4.60	−0.57	0.02*
Maximum glucose day 2	−0.0067	−0.69	0.001*	0.85	0.20	0.26
Corticospinal tract						
Minimum glucose day 3	0.0013	0.07	0.24	−1.08	−0.17	0.17
Maximum glucose day 3	−0.0014	−0.13	0.47	−0.23	−0.07	0.60
Optic radiation						
Minimum glucose day 3	0.0075	0.34	0.10	−3.80	−0.39	0.09
Maximum glucose day 3	−0.0068	−0.54	0.008*	0.31	−0.06	0.60

Table 4
Mean diffusion tensor imaging measures. Mean and standard deviations of fractional anisotropy (FA) and mean diffusivity (MD) of all regions of interest and tracts of the cohort.

	FA	MD (10^{-5} mm^2/s)
Anterior white matter	0.16 ± 0.05	153.16 ± 17.74
Central white matter	0.23 ± 0.07	133.78 ± 17.04
Posterior white matter	0.19 ± 0.06	149.32 ± 23.25
Genu of corpus callosum	0.58 ± 0.14	118.51 ± 30.68
Splenium of corpus callosum	0.68 ± 0.12	107.04 ± 19.44
Caudate	0.08 ± 0.03	118.47 ± 14.71
Lentiform nucleus	0.14 ± 0.03	112.92 ± 9.78
Pulvinar nucleus of thalamus	0.19 ± 0.06	102.40 ± 11.46
Ventrolateral nucleus of thalamus	0.17 ± 0.04	105.66 ± 10.40
Posterior limb of the internal capsule	0.52 ± 0.07	106.74 ± 11.41
Optic radiation	0.29 ± 0.06	135.76 ± 20.55
Calcarine cortex	0.12 ± 0.05	117.04 ± 11.81
Hippocampus	0.13 ± 0.06	118.29 ± 18.47
Corticospinal tract	0.31 ± 0.03	121.50 ± 10.23
Optic radiation tract	0.25 ± 0.04	141.28 ± 16.28

artery pH. When FDR q-values were calculated, no significant associations were found.

4. Discussion

Regional brain injury observed with hypo- and hyperglycemia in neonatal encephalopathy after therapeutic hypothermia has not been previously documented in detail. While few studies exist to date on this topic, most prior studies were limited by intermittent glucose testing, limiting the accuracy of measurement of glycemic extremes. This study uniquely combines advanced techniques of continuous glucose monitoring and regional brain MRI metrics to demonstrate that higher maximum glucose levels on the first day of life were associated with widespread changes in mean diffusivity in the anterior and posterior white matter, splenium of the corpus callosum, lentiform nucleus, pulvinar nucleus of the thalamus, posterior limb of the internal capsule, and optic radiations. No changes were found associated with hypoglycemia.

Understanding the DTI and spectroscopic metrics are important to understanding this study's current findings. The apparent diffusion coefficient, also known as MD, measures the magnitude of diffusion and is rotationally invariant, that is, it does not include the anisotropic diffusion effects (Papadakis et al., 1999). FA represents the degree of anisotropy of a diffusion process, i.e., deviation from isotropic diffusion. FA has been reported to be the best rotationally invariant scalar metric for measuring diffusion anisotropy (Basser et al., 1994; Pierpaoli and Basser, 1996; Pierpaoli et al., 1996). Rotationally invariant anisotropy metrics are advantageous because they are independent of the frame of reference, of the direction of the applied diffusion gradients and of the orientation of the studied structures within the voxels. Changes in MD and FA reflect alteration in the microstructure of the brain. In animal models, it has been demonstrated that acute ischemic brain injury results in decreases in FA and MD, and that reduction in MD values are associated with increased cell death, astrocyte reactivity, and microglial activation in the cerebral cortex (Tuor et al., 2014).

Meanwhile, MR spectroscopy enables measurement of brain metabolites, including NAA, choline, and lactate reported here. NAA includes metabolites found in neuronal mitochondria and indicates neuronal viability, while choline is a component of cell membranes. Lactate is a metabolite of anaerobic metabolism, and thus elevated levels reflect inadequate oxygen supplies relative to energy expenditure needs (Peden et al., 1993).

Investigating hypoglycemia in this current cohort of newborns, where most experienced therapeutic hypothermia, lower minimum glucose level was not associated with any regional changes in brain microstructure. Previous studies of neonatal hypoglycemia showed brain microstructural changes, including low MD values, in the posterior grey matter (including the calcarine cortex), posterior white matter, and pulvinar nucleus of the thalamus (Barkovich et al., 1998; Filan et al., 2006; Tam et al., 2008), with findings of high sensitivity and specificity even in the face of concurrent hypoxia–ischemia (Wong et al., 2013). As well, in the context of hypoxia–ischemia, it has been demonstrated that hypoglycemia is associated with worse corticospinal injury (Tam et al., 2012). One of the key differences between this study and previous studies is that this study comprises a cohort almost entirely managed with therapeutic hypothermia, which may be protective against these microstructural changes. As well, our clinical teams are keenly aware of the potential brain injury associated with hypoglycemia, which manifests as diffusion changes on MRI and has been shown to correlate with apoptosis (Roelants-van Rijn et al., 2001) and neuronal eosinophilic degeneration (Tam et al., 2008) on histopathology. Strict protocols are in place to maintain glucose levels above 2.6 mmol/L, limiting the duration of hypoglycemia. These two factors may contribute to our failure to detect any diffusion changes in the traditionally reported areas.

Surprisingly, lower blood glucose in the first day of life was associated with higher MD values in the optic radiations. While it is surprising that infants with lower minimum glucose demonstrate better metrics of brain microstructure, this may perhaps reflect that infants in this current cohort with lower minimum glucose values may have milder hypoxic-ischemic injury, beyond which we were able to adjust for using 5-minute Apgar scores and umbilical artery pH. As well, as our previous findings were in the pre-hypothermia era, some of the currently observed differences may relate to impacts of therapeutic hypothermia.

Hyperglycemia has only more recently been noted to be associated with poor outcome after neonatal encephalopathy, since the introduction of therapeutic hypothermia (Al Shafouri et al., 2015; Basu et al., 2016; Chouthai et al., 2015; Montaldo et al., 2020). This study provides a novel and detailed view of how high blood sugar relates to regional changes in brain microstructure. Indeed, we demonstrate widespread decreases in MD in the anterior and posterior white matter, corpus callosum, deep grey nuclei, optic radiation, and corticospinal tract associated with higher maximum glucose on the first day of life. It is interesting to note that the regions impacted are traditionally associated with hypoxic-ischemic injury (both basal ganglia and watershed patterns) (Miller et al., 2005), as well as neonatal hypoglycemia. In regards to the traditional HIE injury patterns, hyperglycemia may potentially be additive to worsen brain injury from hypoxia-ischemia, or simply be a sensitive marker for worse hypoxic-ischemic insult. Indeed, worsening traditional brain injury patterns have been previously described to be associated with hyperglycemia (Basu et al., 2018). Adjusting our analyses for 5-minute Apgar scores and umbilical artery pH are attempts at quantitatively adjusting for hypoxia–ischemia severity, suggesting our results are plausible. We have not adjusted for severity of clinical presentation, as degree of clinical encephalopathy is simply a reflection of overall brain injury, and reflects a wide range of etiologies beyond hypoxia–ischemia. It is interesting to note that some regions classically associated with hypoxic-ischemic brain injury, including the ventrolateral nucleus of the thalamus and the hippocampus, were not associated with hyperglycemia. As well, some regions classically associated with hypoglycemia, including the calcarine cortex, was not associated with hyperglycemia. These results thus suggest that hyperglycemia is associated with changes in somewhat different regions from hypoxia-ischemia or hypoglycemia.

In the context of neonatal encephalopathy, diffusion restriction is most commonly considered to be due to cytotoxic edema and a sign of brain injury. However, diffusion restriction can also be seen with myelin edema or neuroinflammation. Animal models of brain injury after hyperglycemia may provide further insight into the possible mechanisms of injury. Isolated hyperglycemia in juvenile rats has been demonstrated to result in increased brain swelling, decreased cortical blood flow and reduced high-energy phosphates (Glaser et al., 2012). In rat models of neonatal HIE, hyperglycemia has been shown to increase neuronal injury (Sheldon et al., 1992). Thus, it is biologically plausible that the changes in brain microstructure observed here associated with hyperglycemia are a result of acute brain injury from hyperglycemia.

No associations were found between glucose levels and regional NAA/Cr, Cho/Cr, or lactate/Cr ratios. The absence of detected associations between hyperglycemia and lactate/Cr ratios also argues against an association between hyperglycemia and worse hypoxic-ischemic insult, supporting the possibility of hyperglycemia being an independent cause of brain injury in this population.

While this study combines meticulous collection of continuous glucose levels and microstructural and metabolic brain imaging metrics, its observational nature precludes the ability to determine causality. Further analyses are needed to answer additional clinically-relevant questions of whether strict control of hyperglycemia can decrease brain injury, and what targets should be for such management. Indeed, our findings suggest that protocols for managing hypoglycemia have improved outcomes, and thus the same could hold true for further efforts to optimize hyperglycemia management. In addition, our MR spectroscopy data is less optimal, with high rates of incomplete studies. However, the findings reported do corroborate with the DTI findings.

Another limitation of this study is the combination of scans at both 3 T and 1.5 T. Signal-to-noise ratio from 3 T is higher than from 1.5 T (Alexander et al., 2006). However, the mean difference of FA and MD values derived from 3 T compared to 1.5 T scanner are relatively small. The mean difference in MD has been estimated at 2.3% ± 3.2% and mean difference in FA has been estimated at 1.2% ± 2.6% (Shaw et al., 2017). Further only a small proportion (16%) of neonates in our cohort were scanner on 1.5 T, and the reasons for doing so were random, related to need for scanning over the weekend and not related to the acuity of the infant's medical condition. Hence, the difference in magnetic field strength of the scanner was unlikely to have a substantial impact or bias on the study findings.

A portion of the study subjects were sedated for MRI using midazolam or chloral hydrate. The study analyses did not consider potential impacts of sedation on imaging metrics. Sevoflurane anesthesia has been shown to result in transient decreases in FA and transient increases in MD (Tang et al., 2021). Further, FA was lower and MD was higher at 100 min than at 40 min post administration of anesthesia. However, there has been no published study assessing the impact of midazolam or chloral hydrate on diffusion parameters. The impact of a short anesthetic or sedation on DTI parameters in this cohort are likely not contributory to the research findings, especially since minimal sedation was used for study success and scan time was limited to just under an hour.

While there are different methods for tractography, in this study we have opted to use the simpler and faster deterministic tractography approach. Probabilistic tractography may be more robust and sensitive for identifying some white matter tracts, particularly smaller tracts, and more robust to partial volume averaging effects and uncertainties in the underlying fiber direction due to imaging noise, but takes longer to compute. In this study, we evaluated two large white matter tractography, corticospinal and optic radiation tractography using deterministic tractography. Deterministic tractography has been used widely in clinical practice and research in neonates and children (Dubner et al., 2019; Ratnarajah et al., 2013; Young et al., 2018). We postulate that deterministic tractography could detect microstructural changes in the corticospinal and optic radiation tractography and correlate with abnormal glucose. Further differences between deterministic and probabilistic tractography of major white matter tracts such as corticospinal tracts have been shown to be minimal (Stefanou et al., 2016).

Another limitation of this study is that the large number of brain regions. Due to the paucity of information in the literature regarding the brain regions implicated with abnormal glycemia (especially hyperglycemia) in the newborn, the goal of this study was to take a fresh and systematic look at brain regional injury associated with glucose variations, and thus multiple regions across the cerebral hemispheres were evaluated. The use of FDR sharpened q-values, instead of traditional p-values, attempts to address some of these limitations.

5. Conclusions

In summary, this study demonstrates a number of important findings relating glucose levels and brain microstructural changes in the era of therapeutic hypothermia for neonatal encephalopathy. Unlike older studies, hypoglycemia was not found to be associated with brain microstructural changes in this cohort treated with therapeutic hypothermia. Hyperglycemia on the first day of life showed strong associations with widespread brain microstructural changes, in regions overlapping but not identical to those impacted by hypoxia–ischemia or hypoglycemia. While causality cannot be determined in this observational study, these findings should help neonatologists and neuroradiologists to better understand the potential contributions of hypoxia–ischemia and abnormal glycemia to brain injury after neonatal encephalopathy with therapeutic hypothermia. While prior studies have demonstrated DTI and MR spectroscopic metrics to be predictive of long-term outcome (Al Amrani et al., 2017; Lally et al., 2019), follow-up of this cohort is in progress, and will be important to determine if these imaging findings translate to long-term outcomes.

CRediT authorship contribution statement

Emily W.Y. Tam: Conceptualization, Formal analysis, Funding acquisition, Investigation, Methodology, Supervision, Writing - original draft. **Daphne Kamino:** Data curation, Investigation, Project administration, Writing - review & editing. **Anwar S. Shatil:** Formal analysis, Investigation, Software, Visualization, Writing - review & editing. **Vann Chau:** Investigation, Methodology, Writing - review & editing. **Aideen M. Moore:** Methodology, Writing - review & editing. **Rollin Brant:** Formal analysis, Writing - review & editing. **Elysa Widjaja:** Investigation, Methodology, Supervision, Writing - review & editing.

Declaration of Competing Interest

The authors declare that they have no known competing financial interests or personal relationships that could have appeared to influence the work reported in this paper.

Acknowledgements

This study was funded by the Canadian Institutes of Health Research [MOP-133710, PJT-166076], the National Institutes of Health [R01 HD101419], and the SickKids Foundation. Continuous glucose monitors were supplied by Medtronic Canada. This study was investigator-led, and the funding agencies had no influence on any aspect of study design, data collection, or interpretation.

References

Al Amrani, F., Kwan, S., Gilbert, G., Saint-Martin, C., Shevell, M., Wintermark, P., 2017. Early imaging and adverse neurodevelopmental outcome in asphyxiated newborns treated With Hypothermia. Pediatr. Neurol. 73, 20–27.

Al Shafouri, N., Narvey, M., Srinivasan, G., Vallance, J., Hansen, G., 2015. High glucose variability is associated with poor neurodevelopmental outcomes in neonatal hypoxic ischemic encephalopathy. J. Neonatal Perinatal Med. 8 (2), 119–124.

Alexander, A.L., Lee, J.E., Wu, Y.-C., Field, A.S., 2006. Comparison of diffusion tensor imaging measurements at 3.0 T versus 1.5 T with and without parallel imaging. Neuroimaging Clin. N. Am. 16 (2), 299–309.

Anderson, M.L., 2008. Multiple inference and gender differences in the effects of early intervention: a reevaluation of the Abrecedarian, Perry preschool, and early training projects. J. Am. Stat. Assoc. 103, 1481–1495.

Auerbach, A., Eventov-Friedman, S., Arad, I., Peleg, O., Bdolah-Abram, T., Bar-Oz, B., Zangen, D.H., 2013. Long duration of hyperglycemia in the first 96 hours of life is associated with severe intraventricular hemorrhage in preterm infants. J. Pediatr. 163 (2), 388–393.

Badawi, N., Kurinczuk, J.J., Keogh, J.M., Alessandri, L.M., O'Sullivan, F., Burton, P.R., Pemberton, P.J., Stanley, F.J., 1998. Antepartum risk factors for newborn encephalopathy: the Western Australian case-control study. BMJ 317 (7172), 1549–1553.

Barkovich, A.J., Ali, F.A., Rowley, H.A., Bass, N., 1998. Imaging patterns of neonatal hypoglycemia. AJNR Am. J. Neuroradiol. 19, 523–528.

Basser, P.J., Mattiello, J., LeBihan, D., 1994. MR diffusion tensor spectroscopy and imaging. Biophys. J. 66 (1), 259–267.

Basu, S.K., Kaiser, J.R., Guffey, D., Minard, C.G., Guillet, R., Gunn, A.J., 2016. Hypoglycaemia and hyperglycaemia are associated with unfavourable outcome in infants with hypoxic ischaemic encephalopathy: a post hoc analysis of the CoolCap Study. Arch. Dis. Child. Fetal Neonatal Ed. 101 (2), F149–F155.

Basu, S.K., Ottolini, K., Govindan, V., Mashat, S., Vezina, G., Wang, Y., Ridore, M., Chang, T., Kaiser, J.R., Massaro, A.N., 2018. Early glycemic profile is associated with brain injury patterns on magnetic resonance imaging in hypoxic ischemic encephalopathy. J. Pediatr. 203, 137–143.

Behrens, T.E.J., Woolrich, M.W., Jenkinson, M., Johansen-Berg, H., Nunes, R.G., Clare, S., Matthews, P.M., Brady, J.M., Smith, S.M., 2003. Characterization and propagation of uncertainty in diffusion-weighted MR imaging. Magn. Reson. Med. 50 (5), 1077–1088.

Carlin, D., Babourina-Brooks, B., Davies, N.P., Wilson, M., Peet, A.C., 2019. Variation of T2 relaxation times in pediatric brain tumors and their effect on metabolite quantification. J. Magn. Reson. Imaging 49 (1), 195–203.

Chau, V., Poskitt, K.J., McFadden, D.E., Bowen-Roberts, T., Synnes, A., Brant, R., Sargent, M.A., Soulikias, W., Miller, S.P., 2009. Effect of chorioamnionitis on brain development and injury in premature newborns. Ann. Neurol. 66 (2), 155–164.

Chouthai, N.S., Sobczak, H., Khan, R., Subramanian, D., Raman, S., Rao, R., 2015. Hyperglycemia is associated with poor outcome in newborn infants undergoing therapeutic hypothermia for hypoxic ischemic encephalopathy. J. Neonatal Perinatal Med. 8 (2), 125–131.

Dubner, S.E., Dodson, C.K., Marchman, V.A., Ben-Shachar, M., Feldman, H.M., Travis, K. E., 2019. White matter microstructure and cognitive outcomes in relation to neonatal inflammation in 6-year-old children born preterm. Neuroimage Clin. 23, 101832. https://doi.org/10.1016/j.nicl.2019.101832.

Filan, P.M., Inder, T.E., Cameron, F.J., Kean, M.J., Hunt, R.W., 2006. Neonatal hypoglycemia and occipital cerebral injury. J. Pediatr. 148 (4), 552–555.

Glaser, N., Ngo, C., Anderson, S., Yuen, N., Trifu, A., O'Donnell, M., 2012. Effects of hyperglycemia and effects of ketosis on cerebral perfusion, cerebral water distribution, and cerebral metabolism. Diabetes 61 (7), 1831–1837.

Godoy, D.A., Di Napoli, M., Rabinstein, A.A., 2010. Treating hyperglycemia in neurocritical patients: benefits and perils. Neurocrit. Care 13 (3), 425–438.

Harris, P.A., Taylor, R., Thielke, R., Payne, J., Gonzalez, N., Conde, J.G., 2009. Research electronic data capture (REDCap)–a metadata-driven methodology and workflow process for providing translational research informatics support. J. Biomed. Inform. 42 (2), 377–381.

Jacobs, S.E., Berg, M., Hunt, R., Tarnow-Mordi, W.O., Inder, T.E., Davis, P.G., 2013. Cooling for newborns with hypoxic ischaemic encephalopathy. Cochrane Database Syst Rev, CD003311.

Lally, P.J., Montaldo, P., Oliveira, V., Soe, A., Swamy, R., Bassett, P., Mendoza, J., Atreja, G., Kariholu, U., Pattnayak, S., Sashikumar, P., Harizaj, H., Mitchell, M., Ganesh, V., Harigopal, S., Dixon, J., English, P., Clarke, P., Muthukumar, P., Satodia, P., Wayte, S., Abernethy, L.J., Yajamanyam, K., Bainbridge, A., Price, D., Huertas, A., Sharp, D.J., Kalra, V., Chawla, S., Shankaran, S., Thayyil, S., Lally, P.J., Montaldo, P., Oliveira, V., Soe, A., Swamy, R., Bassett, P., Mendoza, J., Atreja, G., Kariholu, U., Pattnayak, S., Sashikumar, P., Harizaj, H., Mitchell, M., Ganesh, V., Harigopal, S., Dixon, J., English, P., Clarke, P., Muthukumar, P., Satodia, P., Wayte, S., Abernethy, L.J., Yajamanyam, K., Bainbridge, A., Price, D., Huertas, A., Sharp, D.J., Kalra, V., Chawla, S., Shankaran, S., Thayyil, S., 2019. Magnetic resonance spectroscopy assessment of brain injury after moderate hypothermia in neonatal encephalopathy: a prospective multicentre cohort study. Lancet Neurol. 18 (1), 35–45.

McKinlay, C.J.D., Alsweiler, J.M., Anstice, N.S., Burakevych, N., Chakraborty, A., Chase, J.G., Gamble, G.D., Harris, D.L., Jacobs, R.J., Jiang, Y., Paudel, N., San Diego, R.J., Thompson, B., Wouldes, T.A., Harding, J.E., 2017. Association of Neonatal Glycemia With Neurodevelopmental Outcomes at 4.5 Years. JAMA Pediatr. 171 (10), 972. https://doi.org/10.1001/jamapediatrics.2017.1579.

Miller, S.P., Latal, B., Clark, H., Barnwell, A., Glidden, D., Barkovich, A.J., Ferriero, D.M., Partridge, J.C., 2004. Clinical signs predict 30-month neurodevelopmental outcome after neonatal encephalopathy. Am. J. Obstet. Gynecol. 190 (1), 93–99.

Miller, S.P., Ramaswamy, V., Michelson, D., Barkovich, A.J., Holshouser, B., Wycliffe, N., Glidden, D.V., Deming, D., Partridge, J.C., Wu, Y.W., Ashwal, S., Ferriero, D.M., 2005. Patterns of brain injury in term neonatal encephalopathy. J. Pediatr. 146 (4), 453–460.

Mohammadi, S., Möller, H.E., Kugel, H., Müller, D.K., Deppe, M., 2010. Correcting eddy current and motion effects by affine whole-brain registrations: evaluation of three-dimensional distortions and comparison with slicewise correction. Magn. Reson. Med. 64 (4), 1047–1056.

Montaldo, P., Caredda, E., Pugliese, U., Zanfardino, A., Delehaye, C., Inserra, E., Capozzi, L., Chello, G., Capristo, C., Miraglia Del Giudice, E., Iafusco, D., 2020. Continuous glucose monitoring profile during therapeutic hypothermia in encephalopathic infants with unfavorable outcome. Pediatr. Res. 88 (2), 218–224.

Papadakis, N.G., Xing, D.a., Huang, C.-H., Hall, L.D., Carpenter, T.A., 1999. A comparative study of acquisition schemes for diffusion tensor imaging using MRI. J. Magn. Reson. 137 (1), 67–82.

Parsons, M.W., Barber, P.A., Desmond, P.M., Baird, T.A., Darby, D.G., Byrnes, G., Tress, B.M., Davis, S.M., 2002. Acute hyperglycemia adversely affects stroke outcome: a magnetic resonance imaging and spectroscopy study. Ann. Neurol. 52 (1), 20–28.

Peden, C.J., Rutherford, M.A., Sargentoni, J., Cox, I.J., Bryant, D.J., Dubowitz, L.M., 1993. Proton spectroscopy of the neonatal brain following hypoxic-ischaemic injury. Dev. Med. Child Neurol. 35, 502–510.

Pierpaoli, C., Basser, P.J., 1996. Toward a quantitative assessment of diffusion anisotropy. Magn. Reson. Med. 36 (6), 893–906.

Pierpaoli, C., Jezzard, P., Basser, P.J., Barnett, A., Di Chiro, G., 1996. Diffusion tensor MR imaging of the human brain. Radiology 201 (3), 637–648.

Pinchefsky, E.F., Hahn, C.D., Kamino, D., Chau, V., Brant, R., Moore, A.M., Tam, E.W.Y., 2019. Hyperglycemia and Glucose Variability Are Associated with Worse Brain Function and Seizures in Neonatal Encephalopathy: A Prospective Cohort Study. J. Pediatr. 209, 23–32.

Ratnarajah, N., Rifkin-Graboi, A., Fortier, M.V., Chong, Y.S., Kwek, K., Saw, S.-M., Godfrey, K.M., Gluckman, P.D., Meaney, M.J., Qiu, A., 2013. Structural connectivity asymmetry in the neonatal brain. Neuroimage 75, 187–194.

Roelants-van Rijn, A., Nikkels, P., Groenendaal, F., van der Grond, J., Barth, P., Snoeck, I., Beek, F., de Vries, L., 2001. Neonatal diffusion-weighted MR imaging: relation with histopathology or follow-up MR examination. Neuropediatrics 32 (06), 286–294.

Sánchez Fernández, I., Morales-Quezada, J.L., Law, S., Kim, P., 2017. Prognostic value of brain magnetic resonance imaging in neonatal hypoxic-ischemic encephalopathy: a meta-analysis. J. Child Neurol. 32 (13), 1065–1073.

Saqqur, M., Shuaib, A., Alexandrov, A.V., Sebastian, J., Khan, K., Uchino, K., 2015. The correlation between admission blood glucose and intravenous rt-PA-induced arterial recanalization in acute ischemic stroke: a multi-centre TCD study. Int. J. Stroke 10 (7), 1087–1092.

Shaw, C.B., Jensen, J.H., Deardorff, R.L., Spampinato, M.V., Helpern, J.A., 2017. Comparison of diffusion metrics obtained at 1.5T and 3T in human brain with diffusional kurtosis imaging. J. Magn. Reson. Imaging 45 (3), 673–680.

Sheldon, R.A., Partridge, J.C., Ferriero, D.M., 1992. Postischemic hyperglycemia is not protective to the neonatal rat brain. Pediatr. Res. 32 (4), 489–493.

Slidsborg, C., Jensen, L.B., Rasmussen, S.C., Fledelius, H.C., Greisen, G., Cour, M.d.l., 2018. Early postnatal hyperglycaemia is a risk factor for treatment-demanding retinopathy of prematurity. Br. J. Ophthalmol. 102 (1), 14–18.

Smith, S.M., Jenkinson, M., Johansen-Berg, H., Rueckert, D., Nichols, T.E., Mackay, C.E., Watkins, K.E., Ciccarelli, O., Cader, M.Z., Matthews, P.M., Behrens, T.E.J., 2006. Tract-based spatial statistics: voxelwise analysis of multi-subject diffusion data. Neuroimage 31 (4), 1487–1505.

Stefanou, M.-I., Lumsden, D.E., Ashmore, J., Ashkan, K., Lin, J.-P., Charles-Edwards, G., 2016. Tensor and non-tensor tractography for the assessment of the corticospinal tract of children with motor disorders: a comparative study. Neuroradiology 58 (10), 1005–1016.

Tam, E.W.Y., Ferriero, D.M., Xu, D., Berman, J.I., Vigneron, D.B., Barkovich, A.J., Miller, S.P., 2009. Cerebellar development in the preterm neonate: effect of supratentorial brain injury. Pediatr. Res. 66 (1), 102–106.

Tam, E.W.Y., Haeusslein, L.A., Bonifacio, S.L., Glass, H.C., Rogers, E.E., Jeremy, R.J., Barkovich, A.J., Ferriero, D.M., 2012. Hypoglycemia is associated with increased risk for brain injury and adverse neurodevelopmental outcome in neonates at risk for encephalopathy. J. Pediatr. 161 (1), 88–93.

Tam, E.W.Y., Widjaja, E., Blaser, S.I., MacGregor, D.L., Satodia, P., Moore, A.M., 2008. Occipital lobe injury and cortical visual outcomes after neonatal hypoglycemia. Pediatrics 122 (3), 507–512.

Tang, C.Y., Wang, V.X., Lun, M.Y., Mincer, J.S., Ng, J.C., Brallier, J.W., Schwartz, A.E., Ahn, H., McCormick, P.J., Nir, T., Delman, B., Sano, M., Deiner, S.G., Baxter, M.G., Jiang, Q., 2021. Transient changes in white matter microstructure during general anesthesia. PLoS One 16 (3), e0247678. https://doi.org/10.1371/journal.pone.0247678.

Tuor, U.I., Morgunov, M., Sule, M., Qiao, M., Clark, D., Rushforth, D., Foniok, T., Kirton, A., 2014. Cellular correlates of longitudinal diffusion tensor imaging of axonal degeneration following hypoxic-ischemic cerebral infarction in neonatal rats. Neuroimage Clin. 6, 32–42.

Wilson, M., Reynolds, G., Kauppinen, R.A., Arvanitis, T.N., Peet, A.C., 2011. A constrained least-squares approach to the automated quantitation of in vivo (1)H magnetic resonance spectroscopy data. Magn. Reson. Med. 65 (1), 1–12.

Wong, D.S.T., Poskitt, K.J., Chau, V., Miller, S.P., Roland, E., Hill, A., Tam, E.W.Y., 2013. Brain injury patterns in hypoglycemia in neonatal encephalopathy. AJNR Am. J. Neuroradiol. 34 (7), 1456–1461.

Young, J.M., Vandewouw, M.M., Morgan, B.R., Smith, M.L., Sled, J.G., Taylor, M.J., 2018. Altered white matter development in children born very preterm. Brain Struct. Funct. 223 (5), 2129–2141.